Microwave and millimeter-wave power generation in silicon carbide avalanche devices

I. Mehdi, G. I. Haddad, and R. K. Mains
Department of Electrical Engineering and Computer Science, Solid-State Electronics Laboratory, The University of Michigan, Ann Arbor, Michigan 48109-2122

(Received 3 December 1987; accepted for publication 15 March 1988)

Silicon carbide (SiC), due to its thermal and electronic properties, has long been considered an excellent device material for microwave and millimeter-wave power generation. Numerical simulations were performed to study the typical power generating capabilities of SiC impact avalanche transit-time (IMPATT) diodes utilizing the recent experimental data available. Operating characteristics of double-drift IMPATT devices at 10, 35, 60 and 94 GHz are compared. Both pulsed mode and continuous-wave (cw) mode operation are studied. Finally, a comparison among SiC, Si, and GaAs double-drift IMPATT devices is made at various frequencies. It is shown that, for the pulsed mode of operation, SiC double-drift IMPATT devices can produce significantly higher powers than Si and GaAs devices at comparable frequencies. In the cw mode of operation, SiC devices can produce significantly more power than GaAs devices at all frequencies. However, a comparison at 94 GHz indicates that SiC IMPATT diodes in the cw mode of operation produce power levels comparable to Si IMPATT devices. At lower frequencies the performance of SiC diodes operating in the cw mode is expected to be better than the performance of Si devices due to the better thermal conductivity of SiC.

I. INTRODUCTION

Interest in SiC has resurfaced because of recent advances in material growth techniques. SiC has some material parameters that have an advantage over Si and GaAs devices for high-frequency and high-power applications. SiC has one of the largest reported band gaps of common semiconductors (2.85 eV). Consequently, SiC has a breakdown field which is an order of magnitude higher than the breakdown field of Si or GaAs. The low-field electron and hole mobilities of SiC are smaller than GaAs and Si mobilities, but the saturated electron velocity is higher. The thermal conductivity of SiC is approximately three times larger than the conductivity of Si which means that larger amounts of heat can be dissipated successfully in SiC. These properties could lead to an excellent microwave and millimeter-wave power source. Some researchers have reported device quality SiC growth but the production at best remains very inconsistent.[1–4] Before appreciable resources are dedicated to material growth and characterization, it is important that a thorough study of the theoretical performance of SiC devices be carried out to better understand whether the dedication of resources is justifiable or not. A complete analysis of SiC devices will also permit a comparison between SiC devices and some of the existing device technologies. A preliminary comparison can be made by using some of the general figures of merit (for example, see Ref. 1) but a more complete and accurate understanding can only come from individual device analyses. With this point in mind, the first concrete simulation results for SiC impact avalanche transit-time (IMPATT) diodes are reported here. The device operating characteristics and the typical power generating capabilities of SiC IMPATT diodes are studied at four different operating frequencies, namely, 10, 35, 60 and 94 GHz.

II. MATERIAL PARAMETERS

Silicon carbide can grow in a large variety of polytypes with different structures and properties. The two most common polytypes are the α (hexagonal) and β (cubic) polytypes. Some of the material properties important for IMPATT simulation have been measured for only one polytype and not the other. Since there is no one standard method of growing SiC, most of the material parameters reported differ from one other because of the different quality of the material. It was decided to use the most promising experimental parameters that have been published and furthermore assume that the parameters would not differ substantially from α-SiC to β-SiC. There are still some parameters that have not been measured for any polytype. In this case a reasonable guess was made. These parameters will be measured in the future to further improve the accuracy of the simulation. An illustrative example of such a parameter is the hole saturated drift velocity which is important for double-drift IMPATT device analysis. Since there are no experimental results for this parameter, it was decided to use the same velocity as the one measured for electrons. Table I lists all the material parameters used and the references[4–7] where they were reported.

The velocity-field characteristic for the carriers, obtained from von Muench and Pettenpaul,[5] is expressed as

$$v(E) = v_{sat}(1 - e^{-\mu E/v_{sat}}), \quad (1)$$

where E is the electric field magnitude (in V/cm) and v_{sat}, μ are as given in Table I. Because of the lack of information regarding the diffusion coefficients, the Einstein relationship was used to calculate the diffusion coefficients from the mobility measurements. A constant value for the diffusion coefficients was assumed. The ionization rates at room tempera-

 0021-8979/88/151533-08$02.40 © 1988 American Institute of Physics

TABLE I. Material parameters of silicon carbide (SiC) used for the simulation of double-drift IMPATT structures.

Material parameter	Value	Reference
Electron saturated velocity	2.0×10^7 cm/s	5
Hole saturated velocity	2.0×10^7 cm/s	estimated value
Dielectric constant	9.7	6
Electron mobility	290 cm^2/V s	4
Hole mobility	21 cm^2/V s	4
Electron diffusion constant	9.88	estimated value
Hole diffusion constant	0.546	estimated value
Thermal conductivity	3.87 W/cm K	7

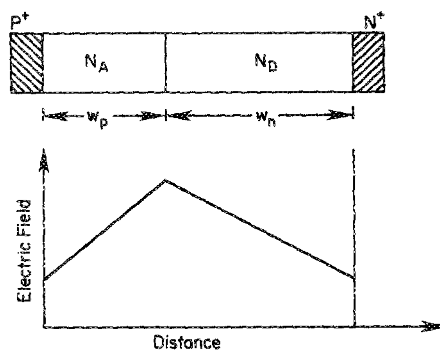

FIG. 1. Doping profile and electric field profile for the simulated double-drift IMPATT structures.

ture for electrons and holes were obtained from Dmitriev *et al.*[8] where different rates were reported depending on whether the applied electric field is oriented parallel to or perpendicular to the *c* axis of the crystal. It was decided to use only one case and the case where the electric field is perpendicular to the *c* axis was selected. The ionization rates used are as follows:

$$\beta_p = 2.54\times10^6 e^{-(1.1\times10^7/E)} \tag{2}$$

and

$$\alpha_n = \beta_p/3.5, \tag{3}$$

where α and β are the ionization rates for electrons and holes, respectively, and are given per centimeter.

III. DEVICE DESIGN AND SIMULATION

Since it is expected that double-drift IMPATT structures can generate more power than their single-drift counterparts, the performance of double-drift IMPATT structures was designed and computed. At each frequency the drift length w_D was chosen as

$$w_D = v(0.74/2f), \tag{4}$$

where v is the particle saturated velocity (assuming equal values for electrons and holes) and f is the operating frequency. Since the same saturated velocity for holes and electrons is assumed, a symmetrical device with $w_n = w_p$ will result. Next, it is assumed that w_D comprises two thirds of the device length so that the total length w is

$$w = \tfrac{3}{2}w_D. \tag{5}$$

The doping concentration was chosen so that at the desired operating current density the electric field at the two contacts would be approximately one third of the maximum electric field which occurs at the *p-n* junction. This design criteria does not have to be achieved rigorously but it should be made certain that the device is always in punch through. Operating current densities were chosen based on previous simulations of Si IMPATT devices at the same frequencies. All simulations were carried out at room temperature.

Details of the device simulation algorithm were described by Bauhahn and Haddad.[9] The drift regions of the device are modeled by use of difference equation versions of the device equations where the carrier velocities, diffusion coefficients (assumed constant in this case), and ionization rates are field dependent.

First, the dc solution was obtained and the doping level was varied until an appropriate electric field profile was achieved. For the ac solution, a sinusoidal rf voltage is impressed across the device so that the terminal voltage as a function of time is given by

$$V(t) = V_{dc} + V_{rf}\sin(2\pi f t). \tag{6}$$

Also, a particular dc bias current density J_{dc} is imposed. Given these constraints, the program iterates until a periodic solution is obtained. At this point the device terminal current waveform is Fourier analyzed; the fundamental component of current together with the sinusoidal voltage component permits calculation of the device efficiency

$$\eta = P_{rf}/P_{dc}, \tag{7}$$

and generated power P_{rf} at the fundamental frequency. The simulation results are normalized per unit area so that P_{rf} is in W/cm^2.

Devices designed with the above-mentioned design rule were simulated at 10, 35, 60 and 94 GHz. It is found that the device efficiencies are considerably lower than the efficiencies obtained from Si and GaAs IMPATT devices at comparable frequencies. The lower efficiencies are not a result of some fundamental material limit, but they result because of a nonoptimum device design. Since the mobility of the holes is considerably lower than the mobility of the electrons, the field in the *p* region is not large enough to cause the holes to travel with the saturated velocity during the whole period of the drift time. Thus, at the end of the rf cycle, while all the electrons have been collected by the contact electrode, there are still holes (and thus charge) left in the device. This physical phenomena results in the degradation of the device efficiency. To correct this nonoptimum design, the *p* region of

TABLE II. Doping densities and device lengths at different frequencies for nonsymmetrical double-drift diodes.

f (GHz)	N_D ($\times10^{16}$ cm^{-3})	W_n (μm)	N_A ($\times10^{16}$ cm^{-3})	W_p (μm)
10	0.7	10.4	1.3	5.6
35	2.2	3.10	5.0	1.6
60	5.0	1.80	9.0	0.9
94	9.4	1.18	17.0	0.6

TABLE III. Operating properties of SiC nonsymmetrical double-drift IMPATT devices at 10 GHz.

V_{rf} (V)	$-G$ (S/cm²)	B (S/cm²)	η (%)	V_{dc} (V)	P_{rf} $\times 10^5$ (W/cm²)	J_{dc} (kA/cm²)	Area $\times 10^{-3}$ (cm²)	P_{rf} (kW 1 Ω)
500	1.80	32.6	10.2	1836	2.25	1.20	1.680	0.38
700	1.47	32.9	16.0	1796	3.60	1.25	1.360	0.49
900	1.13	33.1	21.1	1734	4.60	1.26	1.040	0.48
1000	0.945	33.3	22.7	1698	4.73	1.22	0.854	0.40
1200	0.416	33.9	15.6	1582	2.99	1.21	0.361	0.11
1000	0.091	33.9	13.5	1695	0.454	0.20	0.079	0.01
1000	0.180	33.8	17.6	1697	0.902	0.30	0.158	0.02
1000	0.358	33.7	20.6	1698	1.79	0.51	0.315	0.06
1000	0.746	33.4	22.3	1696	2.73	0.98	0.668	0.25
1000	0.934	33.3	22.7	1698	4.67	1.21	0.843	0.39
1000	1.24	33.0	22.8	1695	6.18	1.60	1.130	0.70
1000	1.57	32.7	22.8	1695	7.84	2.02	1.460	1.14
1000	3.42	30.4	20.4	1664	17.1	5.04	3.670	6.28
1000	4.10	28.3	17.6	1637	20.5	7.14	5.010	10.3
1000	3.93	25.3	12.3	1594	19.6	10.0	6.000	11.8
1000	3.49	23.2	9.24	1584	17.5	11.9	6.320	11.0
1000	3.16	22.3	7.79	1574	15.8	12.9	6.230	9.85
1000	2.21	20.4	4.70	1560	11.0	15.0	5.260	5.80

the double-drift device was made approximately half the value of the n region. Accordingly, the doping of the p region had to be changed so that the field at the contact was still approximately one third of the maximum field. In this way, the holes have to traverse a smaller distance than the electrons. Figure 1 shows the schematic and electric field profile of such a device. Table II shows the doping and device dimensions calculated for nonsymmetrical devices operating at four different frequencies.

As in the case of the symmetrical devices, first a dc solution was obtained which was then used as the starting point for the large-signal ac solution. The results obtained from the ac simulation are presented in Tables III–VI. Each table lists results for a different operating frequency. The first five columns of the tables characterize the operating conditions of the IMPATT devices. For each case, a series of simulations are first presented where V_{rf} is varied but J_{dc} is fixed. V_{rf} is varied until a point is reached where the efficiency of the diode becomes maximum. V_{rf} is then held to this constant value and J_{dc} is varied. J_{dc} is first decreased, then increased from the starting value for each case. The point in doing two sets of simulations is to try to optimize the device efficiency and determine the power generating capabilities of the diodes. However, this indeed does not assure an opti-

TABLE IV. Operating properties of SiC nonsymmetrical double-drift IMPATT devices at 35 GHz.

V_{rf} (V)	$-G$ (S/cm²)	B (S/cm²)	η (%)	V_{dc} (V)	P_{rf} $\times 10^5$ (W/cm²)	J_{dc} (kA/cm²)	Area $\times 10^{-4}$ (cm²)	P_{rf} (W 1 Ω)
300	8.26	400.6	16.2	672	3.72	3.42	0.515	19.1
350	7.39	401.6	19.7	660	4.52	3.49	0.458	20.7
400	6.13	402.3	22.4	643	4.90	3.41	0.378	18.5
425	5.70	404.2	23.2	634	5.15	3.49	0.351	18.1
470	3.57	406.9	18.8	604	3.94	3.46	0.217	8.55
425	0.159	406.7	5.70	631	0.144	0.401	0.010	0.014
425	1.83	405.7	19.8	630	1.65	1.32	0.111	1.83
425	6.32	402.3	23.1	632	5.71	3.92	0.391	22.3
425	8.23	400.8	23.5	631	7.43	5.02	0.512	38.1
425	12.8	396.9	23.2	631	11.6	7.92	0.812	93.9
425	23.2	386.0	22.4	625	21.0	15.0	1.56	326.7
425	27.1	380.7	22.0	622	24.5	17.9	1.86	456.2
425	33.7	368.1	20.1	612	30.4	24.8	2.46	748.8
425	38.4	347.6	16.7	596	34.6	34.8	3.14	1086
425	39.4	335.2	14.9	590	35.6	40.5	3.46	1231
425	37.8	324.7	13.0	581	34.1	45.2	3.54	1208
425	34.6	314.9	10.9	574	31.3	49.8	3.45	1080
425	30.7	303.8	8.82	567	27.7	55.4	3.29	911.0

TABLE V. Operating properties of SiC nonsymmetrical double-drift IMPATT devices at 60 GHz.

V_{rf} (V)	$-G$ (S/cm^2)	B (S/cm^2)	η (%)	V_{dc} (V)	P_{rf} $\times 10^5$ (W/cm^2)	J_{dc} (kA/cm^2)	Area $\times 10^{-4}$ (cm^2)	P_{rf} (W 1 Ω)
150	42.3	1168	10.8	435	4.75	10.0	0.309	14.7
200	35.6	1174	16.3	428	7.13	10.2	0.258	18.4
210	34.2	1175	17.3	427	7.54	10.2	0.247	18.6
275	24.3	1184	22.4	410	9.18	9.80	0.173	15.9
320	10.5	1202	14.1	385	5.37	10.2	0.073	3.89
275	2.65	1202	12.4	408	1.00	1.98	0.018	0.183
275	13.7	1193	21.0	409	5.17	6.03	0.961	4.97
275	23.1	1185	22.1	408	8.74	9.71	0.164	14.4
275	49.5	1162	22.8	409	18.7	20.0	0.366	68.6
275	91.0	1112	21.3	404	34.4	40.1	0.731	252
275	104	1087	20.2	400	39.5	48.8	0.876	346
275	119	1053	18.9	396	44.9	59.9	1.06	476
275	127	1020	17.6	391	47.8	69.5	1.20	572
275	131	967	15.1	384	49.5	85.4	1.37	681
275	133	960	14.9	384	50.2	87.4	1.41	708
275	124	914	12.4	377	46.9	101	1.46	685
275	115	893	10.9	372	43.5	107	1.42	618
275	94.2	844	7.86	365	35.6	124	1.31	465

mum design. In order to truly optimize the design, even more thorough calculations are required. However, the calculations presented do provide a typical and reasonably accurate picture of the device performance.

Figures 2–5 show the large-signal results for the four devices operating at different fundamental frequencies. Table VII gives a summary of the SiC IMPATT diodes when matched to a resistance of 1 Ω. From the simulated results presented in the table, it is noted that large power densities can be obtained at microwave and millimeter-wave frequencies with SiC double-drift IMPATTs. However, as is shown next, there are practical limitations that significantly decrease the power generating capabilities of these diodes, especially at millimeter-wave frequencies.

IV. POWER LIMITATIONS OF IMPATT DIODES

There are two limitations that significantly reduce the power that can be generated from IMPATT devices. First, there is the electronic limitation that comes from the restriction of matching the device impedance to the external circuit impedance and second, the thermal limitation that arises because of maximum safe operating temperature. For pulsed operation, if it is assumed that the duty cycle is so low that

TABLE VI. Operating properties of SiC nonsymmetrical double-drift IMPATT devices at 94 GHz.

V_{rf} (V)	$-G$ (S/cm^2)	B (S/cm^2)	η (%)	V_{dc} (V)	P_{rf} $\times 10^5$ (W/cm^2)	J_{dc} (kA/cm^2)	Area $\times 10^{-4}$ (cm^2)	P_{rf} (W 1 Ω)
100	116	2775	9.37	305	5.78	20.2	0.149	8.65
150	92.4	2793	17.2	299	10.4	20.2	0.118	12.3
170	82.3	2803	20.2	295	11.9	19.9	0.105	12.4
200	64.2	2833	22.0	287	12.8	20.3	0.079	10.3
220	37.9	2870	16.5	277	9.19	20.2	0.046	4.23
200	92.4	2878	10.8	2852	1.85	5.99	0.011	0.206
200	16.4	2872	14.7	2854	3.29	7.85	0.019	0.665
200	32.2	2860	18.8	2856	6.43	12.0	0.039	2.52
200	79.6	2819	22.8	286	15.9	24.4	0.100	15.9
200	117	2785	23.6	287	23.4	34.6	0.150	35.3
200	210	2688	22.8	286	41.9	64.3	0.288	121
200	232	2657	22.3	284	46.4	73.3	0.326	151
200	294	2570	21.5	284	58.7	96.5	0.439	258
200	328	2415	17.7	274	65.6	135	0.552	363
200	336	2288	15.3	269	67.1	164	0.628	421
200	328	2245	14.1	266	65.6	174	0.637	418
200	315	2205	12.9	264	63.0	185	0.634	399
200	248	2057	8.66	257	49.4	222	0.577	285

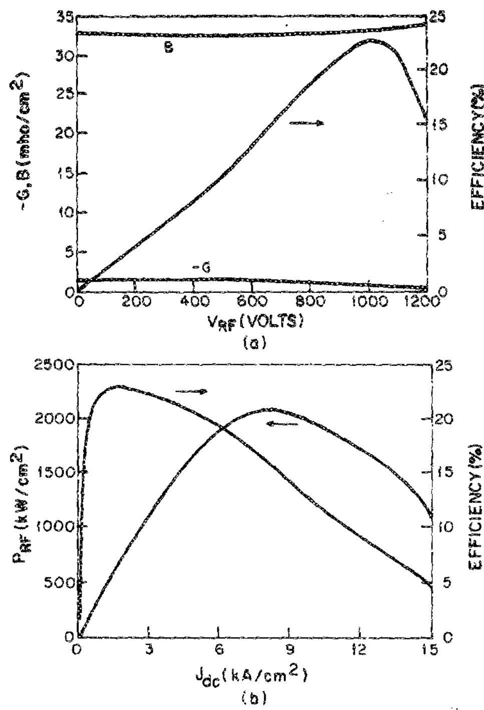

FIG. 2. Large-signal results for a SiC double-drift IMPATT structure at $f = 10$ GHz. (a) $J_{dc} = 1.19$ kA/cm², (b) $V_{rf} = 1000$ V.

appreciable heating does not take place, the electronic impedance matching limitation would ultimately limit the maximum power generated by these devices. For cw operation, the limitations imposed by both considerations are calculated and the smaller value of the power is taken as the typical power expected.

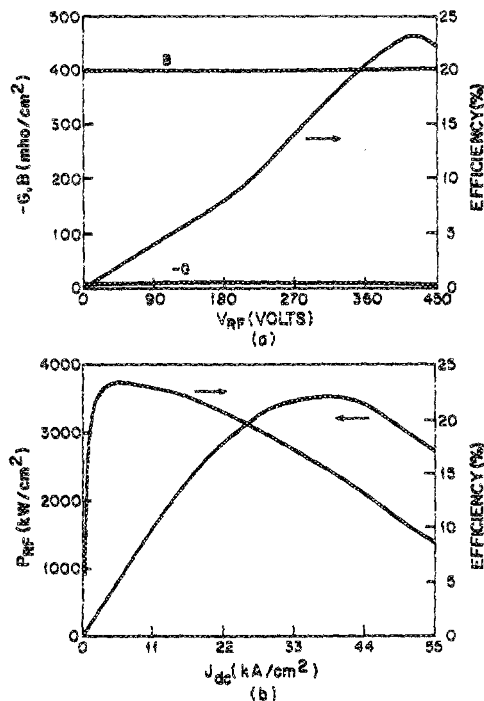

FIG. 3. Large-signal results for a SiC double-drift IMPATT structure at $f = 35$ GHz. (a) $J_{dc} = 3.46$ kA/cm², (b) $V_{rf} = 425$ V.

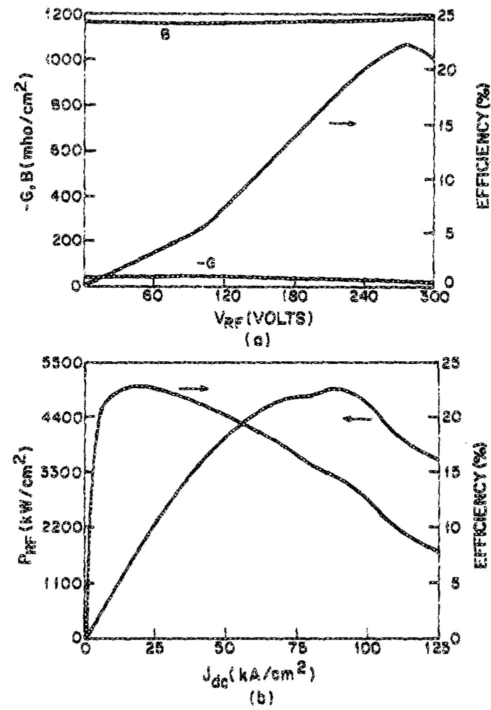

FIG. 4. Large-signal results for a SiC double-drift IMPATT structure at $f = 60$ GHz. (a) $J_{dc} = 9.96$ kA/cm², (b) $V_{rf} = 275$ V.

A. Electronic limitation

The device admittance per unit area at the fundamental frequency is given by $Y = G + jB$. Thus the device reactance can be calculated as

$$X = B/(G^2 + B^2), \tag{8}$$

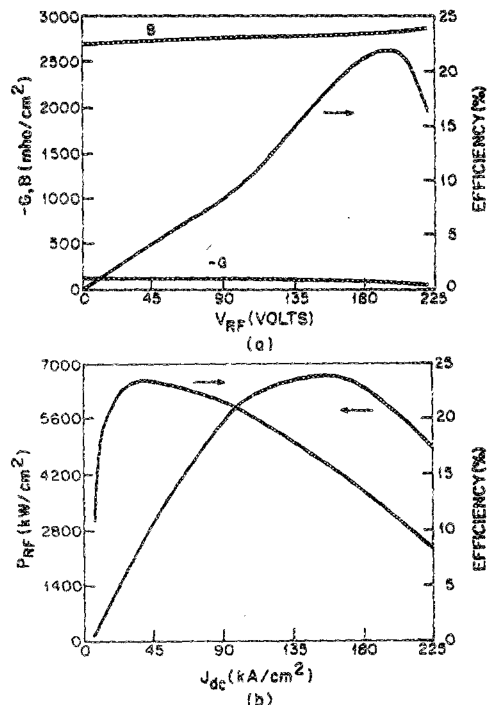

FIG. 5. Large-signal results for a SiC double-drift IMPATT structure at $f = 94$ GHz. (a) $J_{dc} = 19.6$ kA/cm², (b) $V_{rf} = 200$ V.

TABLE VII. Summary of properties of nonsymmetrical double-drift SiC IMPATT device performance when matched to a 1-Ω resistance at different operating frequencies.

Frequency (GHz)	η_{max} (%)	P_{rf} at η_{max} (W 1 Ω)	J_{dc} at η_{max} (kA/cm²)	P_{rf}^{max} (W 1 Ω)	η at P_{rf}^{max} (%)	J_{dc} at P_{rf}^{max} (kA/cm²)
10	23	1140.4	1.46	11800	12	10.0
35	24	93.9	7.92	1230	15	40.5
60	23	68.6	20.0	708	15	87.4
94	24	35.3	34.6	421	15	164.0

and the resistance of the device is

$$R = G/(G^2 + B^2) \tag{9}$$

in Ω cm². To obtain the resistance in ohms, the preceding expression must be divided by the cross-sectional area (A) of the device. If it is assumed that practical circuit considerations limit the diode negative resistance to a minimum magnitude of 1 Ω, then the maximum allowed device area can be found such that $(R/A) = 1$ and thus

$$G/[(G^2 + B^2)A] = 1. \tag{10}$$

The impedance matching consideration sets a lower limit on the allowable magnitude of diode resistance and impedance. If the area were chosen larger, the negative resistance would be smaller than 1 Ω and P_{rf} would be greater, but this will be difficult to match to any practical circuit.

The device area and generated power for the case where the diode exhibits a negative resistance of 1 Ω are given in columns eight and nine of Tables III–VI. It is again noted that large amounts of power can be obtained. However, it should be remembered that these results are for pulsed operation where the heat generated is not a limiting factor. Table VIII gives a summary of the rf power obtainable from double-drift SiC devices at different frequencies (values for Si and GaAs diodes were obtained from Mains and Haddad[10,11]). A comparison is also made with the power values obtained from Si and GaAs. As expected, SiC devices can generate significantly more pulsed power than Si or GaAs devices at all frequencies.

B. Thermal limitation of IMPATT diodes

A proper design requires that the device be able to dissipate the maximum allowed input power without exceeding a maximum allowed temperature. When the diode is operated in a continuous-wave (cw) mode, the thermal properties of the material become very important. In the case of SiC, since large amounts of power are theoretically possible, thermal limitations can become very significant in determining the achievable power densities during cw operation.

TABLE VIII. Comparison of peak electronic rf power (W) obtained at four different frequencies by matching the IMPATT device to a 1-Ω load resistance.

Diode type	Frequency (GHz) 10	35	60	94
SiC uniform double drift	11.8×10^3	1.23×10^3	621	350
GaAs uniform double drift	···	···	122	60.4
Si uniform double drift	···	···	···	24.3

In order to estimate the thermally limited power from the devices, the thermal resistance of the diode must be known. To calculate the thermal resistance of SiC IMPATT diodes an expression is used that has been used successfully for GaAs IMPATT diodes.[10,11] The only change made in the original expression is the substitution of the SiC thermal conductivity value for that of GaAs. For double-drift SiC IMPATT devices, the thermal resistance can then be given approximately by

$$R_{th} = \frac{2}{\pi K_{hs} d} + R_{pkg} + \frac{4 l_1 T_1}{989 \pi d^2} + \frac{4 l_2 T_2}{2322 \pi d^2}, \tag{11}$$

where d is the device diameter (in cm), K_{hs} is the thermal conductivity of the heat sink material (in W/cm K), R_{pkg} is the portion of the thermal resistance due to the package and bonding (in K/W), l_1 is the buffer or substrate thickness (in cm), T_1 is the average temperature of the buffer layer (in K), l_2 is the active layer thickness between the junction and the buffer layer (in cm), and T_2 is the average temperature in the active layer (in K).

The first term is the spreading resistance that occurs at the interface between the diode and the heat sink. It is the result obtained by Kennedy[12] for the case of a uniform current heat flux density incident on a large cylindrical heat sink of thermal conductivity K_{hs}. The third term in the equation, the thermal resistance of the buffer layer of length l_1, can be derived from an expression for thermal resistance, assuming one-dimensional heat flow, given in Olson[13]:

$$R_{th} = \Delta x / KA, \tag{12}$$

where Δx is the length of the section, K is the thermal conductivity, and A is the cross-sectional area. Setting $\Delta x = l_1$ and equating these two terms yields the following expression for the thermal conductivity of SiC in the buffer layer (in W/cm K):

$$K = 989/T_1. \tag{13}$$

The fourth term in the expression represents the thermal resistance of the active layer and is of the same form as the buffer layer term but is reduced by a factor of 0.4. This is because, in deriving the active layer term, uniform heat generation throughout the active region is assumed. Since R_{pkg}

TABLE IX. Summary of continuous wave (cw) rf power (W) for SiC double-drift devices at four different frequencies for mesa and ring structure geometries and different heat-sink materials.

Diode type	Frequency 10	35	60	94
Single mesa, copper heat sink	5.14	2.61	1.74	0.55
Single mesa, diamond heat sink	28.1	11.0	6.03	2.57
Ring structure, copper heat sink	11.9	5.82	2.76	1.58
Ring structure, diamond heat sink	56.20	22.0	11.0	5.23

is very dependent on the packaging and bonding techniques, it is taken to be zero in the thermal resistance calculations. For these calculations, the thermal conductivity of a diamond heat sink is taken as 11.7 W/cm K and that of a copper heat sink as 3.9 W/cm K.

The use of multiple mesas or ring geometries will reduce the first term in the equation as explained in Mains and Haddad.[11] It is assumed here that an improvement of the spreading term by a factor of 0.55 is possible by utilizing geometries more efficient than the single round mesa structure.

Once the thermal resistance expression is known, the diode junction temperature T under large-signal cw conditions is given (in Kelvin) by

$$T = 300 + R_{th}(1-\eta)V_{dc}J_{dc}A, \tag{14}$$

where R_{th} is the thermal resistance, η is the fractional rf generation efficiency, V_{dc} is the diode operating voltage (in V), and J_{dc} is the diode current density (in A/cm^2). For this case it is assumed that $l_1 = 1\ \mu m$ and $T_1 = 725$ K. l_2, of course, depends on the device and T_2 was selected to be 750 K.

From the earlier simulated results it is noted that as the current density is increased the power generated in the device also increases until it reaches a saturated value. However, higher currents also result in large amounts of power being dissipated inside the device which increases the junction temperature. To calculate the maximum amount of current that may be used, Eqs. (10) and (13) are solved simultaneously and the junction temperature is set at $T = 773$ K. It is assumed that this is the maximum allowable temperature for SiC devices. Accepted values for GaAs and Si devices is 500 K, based on the reliability of the contact metals. For SiC devices, using appropriate contact metals, measurements up to 1000 K have been obtained.[7] Equations (10) and (13) are solved in terms of the diode diameter. This places a maximum limit on the area of the diode.

Four different IMPATT cases are analyzed for thermal limitations. In the first case a copper heat sink is used with a single mesa structure. The second case considers a diamond heat sink with a single mesa and the third and fourth cases consider a ring geometry with copper and diamond heat sinks, respectively.

V. cw POWER GENERATION

Two methods of calculating the maximum diode diameter and maximum power generated are now available. One is from impedance matching considerations in which a minimum circuit resistance of 1 Ω is assumed. The second method is from thermal considerations. To estimate the maximum achievable power in practice, the procedure is to calculate the device diameter using both methods and then to choose the smaller of these two values. This procedure has been carried out for the devices under consideration and the maximum achievable cw power is given in Table IX. Table X shows a comparison of SiC, Si, and GaAs diodes operating in the cw mode at different frequencies (values for Si and GaAs diodes are from Mains and Haddad[10,11]). The performance of SiC at lower frequencies is superior to GaAs and Si IMPATT performance. However, at millimeter-wave frequencies, Si devices can produce similar amounts of cw power as the SiC IMPATT devices.

There are two points that should be noted. First, in the thermal resistance calculations it is assumed that the device is operating at 773 K while the results of the room-tempera-

TABLE X. Comparison of cw rf power (W) for various double-drift IMPATT devices with two different heat-sink materials and two different geometries.

Diode Material	f (GHz)	Single mesa: Copper sink	Single mesa: Diamond sink	Ring structure: Copper sink	Ring structure: Diamond sink
Si		...	...	...	...
GaAs	10	0.967	3.93	2.32	5.91
SiC		5.14	12.2	30.3	56.2
Si		...	...	...	...
GaAs	35	...	...	...	...
SiC		2.61	11.0	5.82	22.0
Si		...	...	...	...
GaAs	60	0.19	1.18	0.63	1.8
SiC		1.74	6.03	2.76	11.0
Si		0.69	3.28	1.69	5.94
GaAs	94	0.03	0.18	0.10	0.18
SiC		0.55	2.57	1.58	5.23

ture simulations are used. This was done because there is not enough information to correctly predict the material parameters at 773 K. Since, in general, device performance degrades with increasing temperature, the cw results are perhaps a bit optimistic. Second, the electric field in these structures gets extremely high and there might be some possibility of tunneling. This was not incorporated into the simulation. Again, this could result in different device operating conditions.

VI. CONCLUSIONS

SiC double-drift IMPATT diodes were simulated at 10, 35, 60, and 94 GHz using available material parameters. In the pulsed mode, the SiC IMPATT performance was found to be far superior to the Si and GaAs IMPATT performances. In the cw mode, the performance of SiC devices is superior to GaAs devices especially at lower frequencies. A comparison at 94 GHz between SiC and Si double-drift avalanche diodes indicates that the performance of both materials is comparable. However, it is expected that at lower frequencies the performance of SiC devices will be superior to the Si devices operating in the cw mode due to the better thermal conductivity of SiC. Therefore, significantly improved power levels may be expected from SiC double-drift IMPATTs used in the pulsed mode, but thermal considerations severely limit the power available for cw operation at millimeter-wave frequencies.

ACKNOWLEDGMENT

This work was supported by the National Aeronautics and Space Administration under Grant No. NAG 3-618.

[1] J. D. Parsons, R. F. Bunshah, and O. M. Stafsudd, Solid State Technol. **28**, 133 (1985).
[2] R. F. Davis and H.H. Stadlemaier, "Fundamental Studies of Growth, Doping and Transformation in Beta Silicon Carbide," Technical Report No. 243-043-006, North Carolina State University (1985).
[3] B. C. Johnson, J. M. Meese, G. W. Zajac, J. O. Schreiner, J. A. Kaduk, and T. H. Fleisch, Superlattices and Microstructures **2**, 223 (1986).
[4] S. Nishinio, J. A. Powell, and J. A. Will, Appl. Phys. Lett. **42**, 460 (1983).
[5] W. von Muench and E. Pettenpaul, J. Appl. Phys. **48**, 4823 (1977).
[6] L. Patrick and W. J. Choyke, Phys. Rev. B **2**, 2255 (1970).
[7] E. A. Burgemeister, W. von Muench, and E. Pattenpaul, J. Appl. Phys. **50**, 5790 (1979).
[8] A. P. Dmitriev, A. O. Konstantinov, D. P.Litvin, and V. I. Sankin, Sov. Phys. Semicond. **17**, 686 (1983).
[9] P. E. Bauhahn and G. I. Haddad, IEEE Trans. Electron Devices **ED-24**, 634 (1977).
[10] R. K. Mains and G. I. Haddad, in *Infrared and Millimeter Waves*, edited by K. J. Button (Academic, New York, 1983), Vol. 10.
[11] R. K. Mains and G. I. Haddad, "Properties of High-Efficiency X-Band GaAs IMPATT Diodes," Technical Report No. AFWAL-TR-81-1066, Electron Physics Laboratory, The University of Michigan (1981).
[12] D. P. Kennedy, J. Appl. Phys. **31**, 1490 (1960).
[13] H. M. Olson, IEEE Trans. Electron Devices **ED-23**, 484 (1976).